

# An electro-thermal SPICE model for Reverse Conducting IGBT: simulation and experimental validation

M. Riccio, M. Tedesco, P. Mirone, G. De Falco, L. Maresca, G. Breglio and A. Irace

Department of Electrical Engineering and Information Technologies

University of Naples Federico II

Via Claudio 21, Naples 80125, Italy

michele.riccio@unina.it

**Abstract**—The compact SPICE modeling of Reverse Conducting IGBTs is presented in this paper. The proposed approach is based on a quasi-2D formulation with the joint use of IGBT and PiN diode sub-circuits. Lateral currents paths and turn-on forward delay are considered into the model. Self-heating effect for both IGBT and diode regions is taken into account, enabling reliable electro-thermal analysis. The model is calibrated to fit experimental data of a commercial 20 A – 1.2 kV rated device. As a compelling example to prove the effectiveness of the model, the results of an electro-thermal simulation on a quasi-resonant converter are compared with experiments.

**Keywords** — Reverse Conducting IGBT, SPICE model, electro-thermal, quasi-resonant converter.

## I. INTRODUCTION

In the recent past it has been reported that the reverse conducting IGBTs (RC-IGBTs) are becoming the most suitable choice as bidirectional power switch for low and medium power inverter applications. This result is ascribable to an increased power density in IGBT modules and a reduced packaging, bonding, and silicon costs in fabrication. Nevertheless, due to difficulty to optimize the same design for both IGBT and diode operation, a high reverse recovery current and switching losses are responsible of RC-IGBT devices limitation to soft switching applications. Recently, an innovative design [1] has brought a significant improvement in the electrical behavior in both soft and hard switching conditions, ensuring an increased diffusion in the applications [2]. Consequently, a useful compact model for circuit simulators becomes very attractive from the application point of view. At present time, a SPICE model for RC-IGBT is not present neither in PSPICE nor in other SPICE simulator. The only solution consists to simulate a parallel of an IGBT and a diode, neglecting the internal interaction.

In this paper we propose a methodology for the SPICE modeling of RC-IGBTs, including lateral interaction between IGBT and the diode regions. The aforementioned model describe the primary snapback phenomenon and lateral turn-on dynamic. In addition, the self-heating effect is also taken into account enabling the possibility of electro-thermal simulation using ad-hoc equivalent thermal networks [3].

## II. MODEL DESCRIPTION

In Fig. 1 it is depicted the basic schematic structure of a RC-IGBT. A resistive network, responsible of the initial snapback phenomenon [4], is also shown together with the

corresponding electron current path. Due to the intrinsic bi-dimensional (2D) device structure, the electrical behavior could not be modeled with a mathematical 1D approach. To reduce the complexity growth in the compact device description, the approach proposed in this work is based on a quasi-2D formulation, derived from a coupling of properly modified IGBT and diode sub-circuits.

The structure of the developed SPICE model is depicted in Fig. 2a. The voltages of the input thermal nodes correspond to the temperature increase for both IGBT and diode sides. All the physical quantities used into the model are temperature dependent. As visible in the schematic of Fig. 2a, the IGBT and diode sub-circuits were connected using their internal nodes to reproduce the physics structure of an RC-IGBT. Referring to a structure with a buffer-layer at the collector side, a resistor  $R_{BUF}$  can be used to describe a lateral electron current flow [4]. The resistor value can be expressed as [5]:

$$R_{BUF}(T) = \frac{L_p(L_p + L_N)}{\mu_n q N_B A W_B} \left( \frac{T}{T_0} \right)^\beta \quad (1)$$

where the transversal dimension  $L_Z$  is evaluated using the device area and the lateral length  $L_p + L_N$ . Another connection is present between nodes  $D$  and  $J$ , where a non-linear resistor  $R_{MOD}$  takes into account a transversal current path into the epi-layer. The following expression, function of the base charge  $Q_B$  can be used [6], where the longest transversal current path ( $L_p$ ) has been assumed in order to take into account the worst-case condition:

$$R_{MOD}(T) = \frac{L_p^2}{\mu_n Q_n + (\mu_n + \mu_p) Q_B} \quad (2)$$

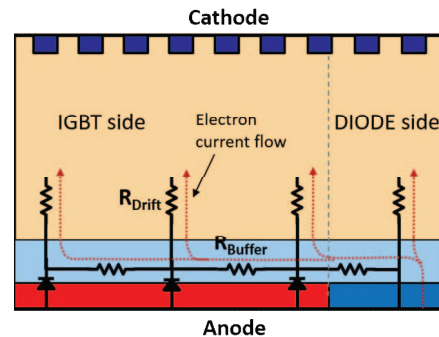


Fig. 1 Simplified internal structure for an RC-IGBT, with electron current path on a resistive distributed network.

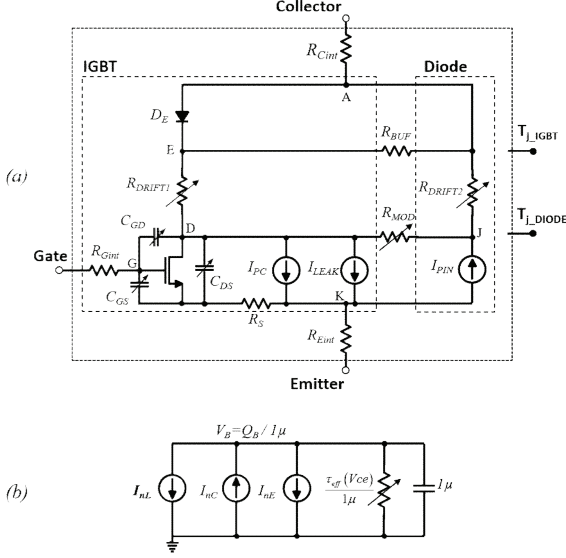


Fig. 2 (a) Developed SPICE circuit, with electrical and thermal nodes. (b) Charge stored sub-circuit for IGBT region, modified to take into account lateral current path from the diode side.

being  $Q_n = qAN_BW$  the background mobile carriers base charge. Its temperature dependence is accounted through the carrier mobility and  $Q_B$ .

The IGBT is described with an optimized version of the model presented in [7], in which the use of explicitly evaluated solution for steady-state carriers charge  $Q_{b0}$ , linear-region transconductance gain factor  $K_F$  and avalanche multiplication factor  $M_{AV}$  were used. A further improvement has been introduced and involves the definition of an effective carrier lifetime ( $\tau_{eff}$ ) that is function of the high-level lifetime in the drift-region ( $\tau_{HL}$ ) and low-level lifetime in the buffer-layer ( $\tau_{BF}$ ). Considering that the IGBT tail current is determined by the carrier recombination in the low doped epi-layer and in the high doped buffer layer together with the injection of electron current into the emitter, it is possible to assess that  $\tau_{eff}$  depends on the external voltage through the extension of the depletion region [8]. To fit the dependence of  $\tau_{eff}$  from the  $V_{ce}$ , the following empirical expression was introduced:

$$\tau_{eff}(T, V_{ce}) = [(\tau_{HL} - \tau_{BF}) \exp(-\delta_\tau V_{ce}) + \tau_{BF}] (T/T_0)^{\beta_\tau} \quad (3)$$

$\delta_\tau$  is the decay rate of  $\tau_{eff}$ , while the temperature dependence is accounted with the model parameter  $\beta_\tau$ .

TABLE I. RC-IGBT STRUCTURE PARAMETERS FOR TCAD SIMULATION

Symbol	Quantity	Value
$L$	Total length	400 $\mu\text{m}$
$L_P$	IGBT length	345 $\mu\text{m}$
$L_N$	Diode length	55 $\mu\text{m}$
$W$	Epi-layer thickness	100 $\mu\text{m}$
$W_B$	Buffer thickness	1.5 $\mu\text{m}$
$N_{epi}$	Epi-layer doping concentration	$1 \times 10^{14} \text{ cm}^{-3}$
$N_B$	Buffer doping concentration	$5 \times 10^{16} \text{ cm}^{-3}$
$p_i$	Cell pitch	5 $\mu\text{m}$

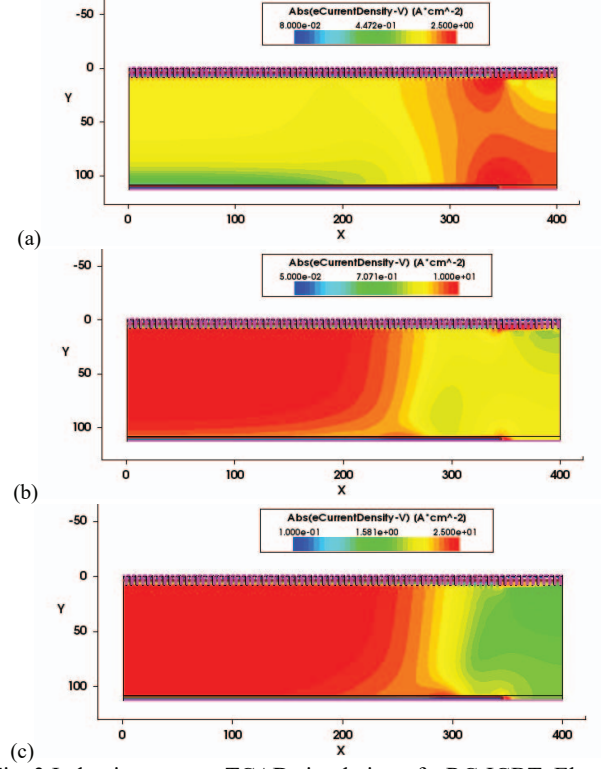


Fig. 3 Inductive turn-on TCAD simulation of a RC-IGBT. Electron current distribution: (a)  $t = 0.5 \mu\text{s}$ ; (b)  $t = 1 \mu\text{s}$ ; (c)  $t = 1.5 \mu\text{s}$ .

However, the significant difference between IGBT and RC-IGBT is that the latter device behaves as a Power MOSFET until the  $P^+_{collector} / N^+_{buffer}$  junction, initially reverse biased, is turned-on when the voltage drop produced by the electron current reaches a sufficient value. This behavior is experimentally evident on the I-V output characteristic that shows a snapback on the collector voltage. The presence of the MOSFET parallel path influences also the dynamic turn-on performances of the device. To this purpose, the turn-on behavior of an RC-IGBT is investigated by means of 2D multicellular TCAD simulations. The structure was designed with reference values reported in literature and that are listed in Table 1. Simulations were performed for the analysis of inductive turn-on and results are reported in Fig. 3 in terms of electron current distribution. These results have shown that, in order to replicate the correct behavior of the RC-IGBT, additional modifications must be included in the original base charge sub-circuit. Referring to the circuit in Fig. 2a, the initial electron current, flowing into  $R_{BUF}$  and in the MOSFET ( $I_{nC}$ ), should not contribute to the collected hole current ( $I_{pC}$ ) and to the modulation of  $R_{DRIFT1}$  through the base-charge  $Q_B$ . To take into account this effect, a further current generator,  $I_{nL}$ , was added to the base-charge sub-circuit as showed in the schematic of Fig. 2b:

$$I_{nL} = I_{RBUF} + I_{RMODN} \quad (4)$$

In Fig. 4 it is reported the static forward output characteristic of the SPICE model for different junction temperatures. The model parameters were set to standard reference values, while for the  $R_{BUF}$  resistance a value to have a non-snapback-free device was used.

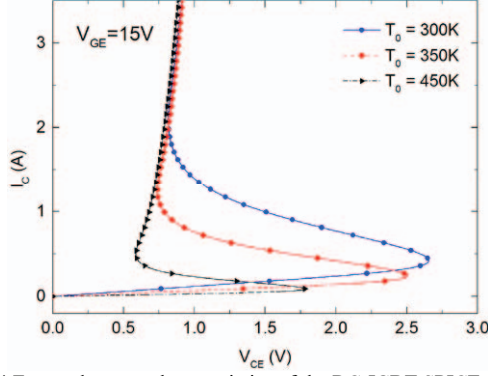


Fig. 4 Forward output characteristics of the RC-IGBT SPICE model function of temperature at  $T_0 = 300$  K,  $T_0 = 350$  K and  $T_0 = 450$  K.

As expected from the theory, the snapback voltage reduces with temperature, as well as the snapback current [9]. The second modification in the model is needed to take into account the forward recovery delay. For this reason, the voltage drop  $V_{epi}$  on the conductivity-modulated epi-layer region of the IGBT should not depend instantaneously on the base-charge  $Q_B$  [10]. In the proposed model, the non-linear resistors  $R_{EPI1}$  and  $R_{MOD}$  are functions of a quantity  $Q_{Bd}$  computed according to the following equation:

$$\tau_F \frac{dQ_{Bd}}{dt} + Q_{Bd} = Q_B \quad (5)$$

In this way, the turn on dynamic is modelled with the time constant  $\tau_F$ .

The diode electric model used for the RC-IGBT is based on the moment-matching approximation of the ambipolar diffusion equation and follows the implementation proposed in [11]. However, in our case the model is provided of four terminals: *anode*, *cathode*, an internal node (into the epi-layer, after the  $p^+n^-$  junction) and temperature increase.

### III. MODEL VALIDATION

The model was validated with measurements on a device manufactured by Infineon Technologies. It is a 20 A – 1.2 kV rated device (IHW20N120R3) designed for resonant converters and soft-switching applications. The developed SPICE model was calibrated on experimental data using a two-steps calibration procedure. At first stage, the IGBT and diode sub-circuits were fitted separately to experimental data. The second step consists to optimize the full RC-IGBT model by means of a best fitting procedure starting from the parameters obtained from the previous step [12]. The  $R_{BUF}$  and  $R_{MOD}$  values can be calibrated using the static  $I_C$ - $V_{CE}$  characteristics and inductive IGBT turn-on measurements.

Fig. 5 shows the experimental and simulated transfer characteristics for different junction temperatures. Fig. 6 reports the output characteristics at room temperature and 425 K, respectively. It can be seen the excellent agreement between SPICE model curves and experimental data. In Fig. 7 the SPICE forward diode I-V curves are compared with measurements, for different temperatures. The results confirm that the model can correctly predict the diode electrical behavior. The dynamic characterization was completed with an inductive turn-on transient reported in Fig. 8.

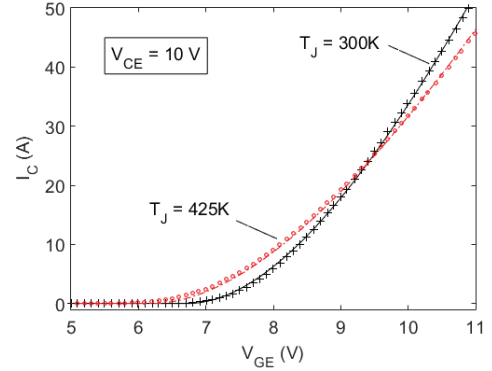


Fig. 5 Transfer characteristics at different temperatures from SPICE simulations (solid lines) and measurements (symbols);  $V_{CE} = 10$  V.

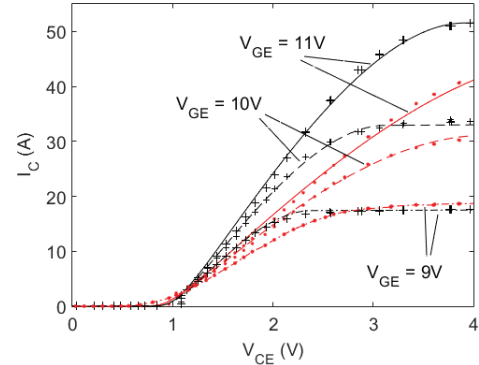


Fig. 6 Output characteristics at different temperature:  $T_0 = 300$  K (black),  $T_0 = 425$  K (red). Solid lines SPICE model; scattered lines experiments.

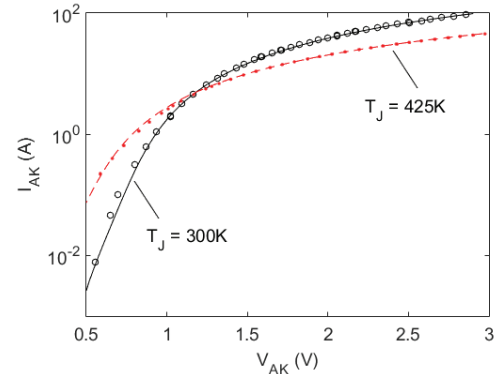


Fig. 7 Forward diode static curves depending on the junction temperature: solid lines SPICE model, scattered lines experiments.

In order to show that the proposed model can replicate the electro-thermal behavior of the RC-IGBT in a real application, a DC-AC converter has been realized using a quasi-resonant converter topology [13]. The schematic of the used circuit is shown in Fig. 9. A 50 kHz switching frequency with a duty cycle of 70% was chosen for the circuit prototype. The resulting regime waveforms are shown in Fig. 10. The DUT steady-state temperature, measured with a thermocouple, reaches about 368 K. To perform an electro-thermal simulation [14], two equivalent thermal networks were used to simulate the self-heating effect within the device (Fig. 9b). The time-constant values for the thermal networks were obtained from the DUT data-sheet.

